

# Kinetics of Low Pressure CVD Growth of SiO<sub>2</sub> on InP and Si

R. Iyer and D. L. Lile

Department of Electrical Engineering, Colorado State University, Fort Collins, Colorado 80523

## ABSTRACT

The kinetics of the low pressure CVD growth of SiO<sub>2</sub> from SiH<sub>4</sub> and O<sub>2</sub> have been studied for an indirect (remote) plasma process. Homogeneous (gas phase) and heterogeneous operating ranges were identified and within the heterogeneous (surface reaction dominated) range of operation the process was found to be very reproducible and consistent. The kinetic rate equation for the growth at 14W RF power input and 400 mtorr total pressure, on both InP and Si substrates, was found to be

$$DR(\text{\AA}/\text{min}) = 1.4 \times 10^{13} \exp\left(\frac{-4227}{T}\right) (n_{\text{O}_2})^{0.5} (n_{\text{SiH}_4})^{1.6}$$

where the  $n$  give the molar flow rate of the constituents for the reaction.

Chemical vapor deposition (CVD) is a technique of considerable importance in the electronics industry not only because of its good controllability but also because of its potential for high purity growth and high throughput. Low pressure CVD processing in particular has attracted much attention because of its capabilities for depositing highly uniform layers over large substrate areas. Typical thermal CVD processes, where heat energy is employed to promote the reaction of the component gases, typically require temperatures in excess of ~350°C which, although much below the ~1000°C employed for the thermal oxidation of Si, is still considered to be quite high when redistribution of impurities due to diffusion must be minimized in, for example, the fabrication of small dimension devices. Compound semiconductor technology also requires low reaction temperatures to retard loss of the more volatile components. To achieve reduced process temperatures, alternate forms of input energy such as RF (1) and microwave plasma discharges (2) as well as photoenhancement have been employed (3).

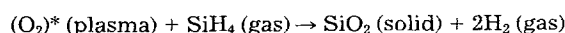
For none of these CVD processes however, and in particular for none of the newer photo- and plasma-enhanced processes, does much information exist in the literature on the kinetics of the growth processes involved. Some data have certainly been published, and most likely, in all fabrication facilities, the performance of CVD reactors is well documented. Notwithstanding these empirical evaluations however, little systematic data exist in the literature on the details of this type of growth so that predictions of deposition parameters can be made.

This paper presents the results of a study of the kinetics of the growth of insulating layers of SiO<sub>2</sub>, from the reaction of SiH<sub>4</sub> and O<sub>2</sub>, on substrates of InP and Si. The CVD growth process employed is a low pressure indirect plasma enhanced reaction where the plasma discharge is created in a region remote from the substrate (4). In this way, as has been previously shown, the potentially damaging effects of the hostile plasma environment on the semiconductor substrate are largely eliminated (5) while at the same time the benefits of the more conventional "direct" plasma process, including reduced growth temperatures, are retained.

Figure 1 shows a schematic of this growth scheme where an oxidant, in this case O<sub>2</sub>, is first passed through a plasma discharge and then on into the reaction vessel where the O<sub>2</sub> products are combined with the silane. In this way growth of SiO<sub>2</sub> has been reported at temperatures as low as 300 K although with some sacrifice in mechanical properties at the very lowest temperatures.

## Experimental

A horizontal hot wall CVD reactor as shown in Fig. 2 has been utilized, in conjunction with a remote plasma chamber, to deposit layers of silicon dioxide on single crystal (100) oriented substrates of Si and InP. The overall reaction for the process is as follows



where the asterisk identifies an excited state of the oxygen resulting from the plasma discharge. Research grade oxygen obtained from Air Products, together with a small quantity of nitrogen to enhance the plasma reaction, is passed through a Pyrex tube of 7.6 cm diam and 17 cm length. These gases are inductively excited by means of a 13.56 MHz power source, capable of delivering up to 200W, and are then routed into the reaction chamber where they are mixed with 5.1% silane diluted in N<sub>2</sub> resulting in growth of the SiO<sub>2</sub> films. The distance between the plasma chamber and the substrate is ~70 cm which we believe is sufficient to allow removal of all the ionized species by collision with the grounded stainless steel connecting tubing. The quartz growth chamber is 11.5 cm in diameter and 63.5 cm in length, dimensions which, together with the flow rates employed, resulted in a Reynolds number for our system ~1, sufficiently below the value of ~2100 typically associated with turbulent flow to presumably ensure laminar conditions in the reactor. Such nonturbulent flow is mandatory for consistent and reproducible results and for

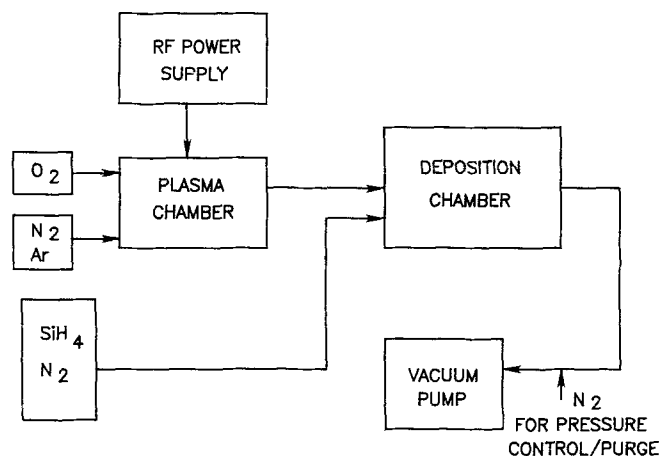


Fig. 1. Block diagram of the indirect plasma enhanced CVD deposition system.

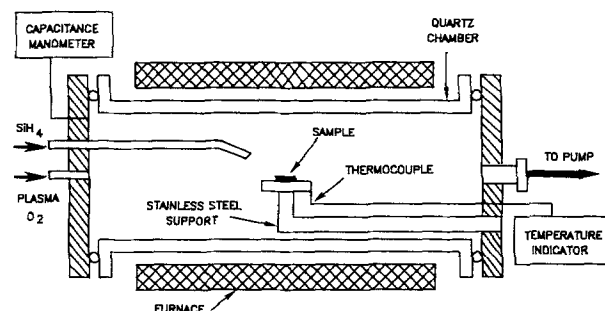


Fig. 2. Schematic of deposition chamber

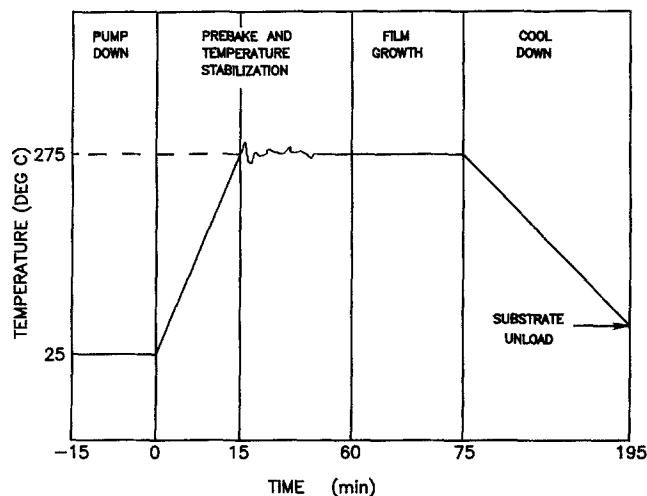


Fig. 3. Typical experimental growth sequence for  $\text{SiO}_2$  deposition

good layer uniformity. The chamber was heated by a 5 kW single zone furnace over a length of 30.5 cm. Two stainless steel flanges sealed with silicone rubber O-rings provide access at one end of the chamber for the reactant gases and at the other end for the vacuum pumping port. Maximum layer uniformity was found to be achieved by introducing the  $\text{SiH}_4$  close to the substrate as shown in Fig. 2, by means of a 1/4 in. diameter pipe, while all other gases entered directly through the end plate. The vacuum was provided by a 12.75 liter/s corrosion resistant rotary pump. Pressure was measured using a capacitance manometer (MKS Baratron), and the temperature of the stainless steel substrate support was monitored by a type K thermocouple. A differentially pumped Balzers quadrupole mass spectrometer sampled gases at the chamber outlet and was used to analyze and control the gas environment in the growth chamber. Initial use of the system showed that growth of  $\text{SiO}_2$  on the Si or InP was largely absent due apparently to consumption of the reactants by a catalytic reaction at the stainless steel substrate support. However, once a coating of  $\text{SiO}_2$  was built up on the substrate support, this effect appeared to be eliminated. Pressure in the deposition chamber was controlled by introducing  $\text{N}_2$  to the inlet of the pump which also increases safety by acting as a continuous purge for the  $\text{SiH}_4$ . The flow rates of the gases were adjusted using needle valves and were measured by means of rotameters. The process sequence was controlled by a TYLAN 16 programmable sequencer and pneumatic valving. Films grown in this system were evaluated for thickness and refractive index by means of a Gaertner Ellipsometer operating at the He-Ne laser wavelength of 6328Å.

The growth cycle for a typical deposition run is shown in Fig. 3. The wafers were cleaned with acetone, rinsed in DI water, cleaned ultrasonically in methanol, rinsed sequentially in methanol and DI water, exposed to xylene vapors followed by a DI water rinse, immersed in HF for 20s, and finally rinsed in DI water and blown dry in nitrogen. The wafers were then immediately loaded into the chamber which was continually purged with UHP  $\text{N}_2$  between runs. Prior to growth the chamber was evacuated to a base pressure of  $\sim 1 \times 10^{-2}$  torr and then purged with UHP  $\text{N}_2$  for ap-

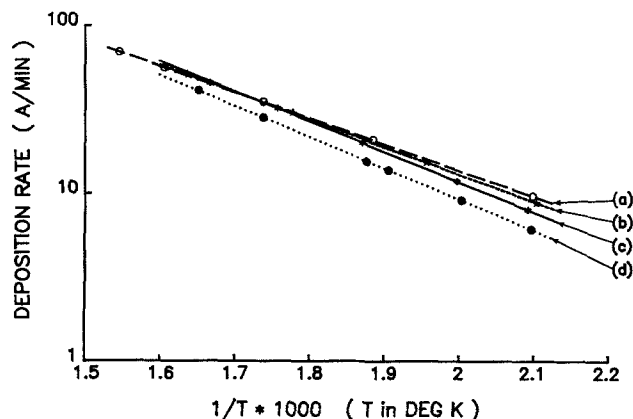


Fig. 4. Arrhenius plot of deposition rate. Chamber pressure = 400 mtorr, nitrogen flow rate =  $21.45 \text{ cm}^3/\text{min}$ , oxygen flow rate =  $12 \text{ cm}^3/\text{min}$ , silane flow rate =  $1.28 \text{ cm}^3/\text{min}$ . Curve (a): Si substrate, RF power: 23W. Curve (b): InP substrate, RF power: 14W. Curve (c): Si substrate, RF power: 14W. Curve (d): Si substrate, RF power: 33W.

proximately 15 min. Following this, the desired deposition pressure was set by adjusting the  $\text{N}_2$  flow to the pump, and the temperature of the reaction chamber was raised and maintained for about an hour for stabilization and bakeout. The purging  $\text{N}_2$  was then turned off, and the reactant gases, silane and oxygen, mixed with a small amount of nitrogen, were introduced. Plasma power was then turned on and the RF-matching network located between the RF generator and the plasma chamber was adjusted to obtain a maximally bright glow. The reactant gases and the furnace were turned off once deposition was complete. UHP  $\text{N}_2$  was then introduced for purging and the system allowed to cool for about 2h at which point the wafers were unloaded.

## Results

Using the CVD system described in the preceding section we have grown a number of layers of  $\text{SiO}_2$  on both InP and Si (100) oriented substrates while maintaining all growth parameters constant, except for one, which was then varied in some systematic manner. Figure 4 illustrates this, where deposition rate as a function of inverse temperature is plotted at various plasma powers for constant silane, oxygen, and nitrogen flow rates for growth on both InP and Si substrates. For all of these experiments the total pressure in the chamber was maintained at 400 mtorr and gas flow rates are as given. In fact, except as otherwise noted, these same values were maintained for all of the experiments reported in this paper. From these data the activation energy for the Si substrate at an RF power input of 14W was calculated to be  $8.4 \pm 0.6 \text{ kcal/mol}$  ( $0.37 \pm 0.026 \text{ eV}$ ) and is seen not to vary significantly with either the type of substrate or the power input. This value is similar to the activation energy for the thermal low pressure CVD silane-oxygen reaction which has previously been reported (6) to be  $\sim 10 \text{ kcal/mol}$  (0.4 eV).

Unless otherwise indicated, all the data shown in this paper are for an oxygen plasma containing  $3.3 \text{ cm}^3/\text{min}$  of nitrogen. Table I shows the deposition rate for various gas mixtures at the inlet to the plasma chamber. Although, and as will be discussed in a later section, additional ef-

Table I. Dependence of  $\text{SiO}_2$  growth rate and refractive index on gas composition in plasma chamber. Silane flow rate =  $1.28 \text{ cm}^3/\text{min}$ , chamber pressure = 400 mtorr, temperature =  $253^\circ\text{C}$

Gases to the plasma chamber			Silicon substrate		InP substrate	
Oxygen flow rate $\text{cm}^3/\text{min}$	Nitrogen flow rate $\text{cm}^3/\text{min}$	Argon flow rate $\text{cm}^3/\text{min}$	Deposition rate $\text{Å}/\text{min}$	Refractive index (n)	Deposition rate $\text{Å}/\text{min}$	Refractive index (n)
11.6	3.3	0.0	20	1.4674	19	1.45970-1.4765
11.6	6.3	0.0	20.2	1.4653	—	—
11.6	0.0	3.0	5.1	1.3787	10.3	1.1831
11.6	0.0	0.0	4.7	1.3798	9.5	1.1870

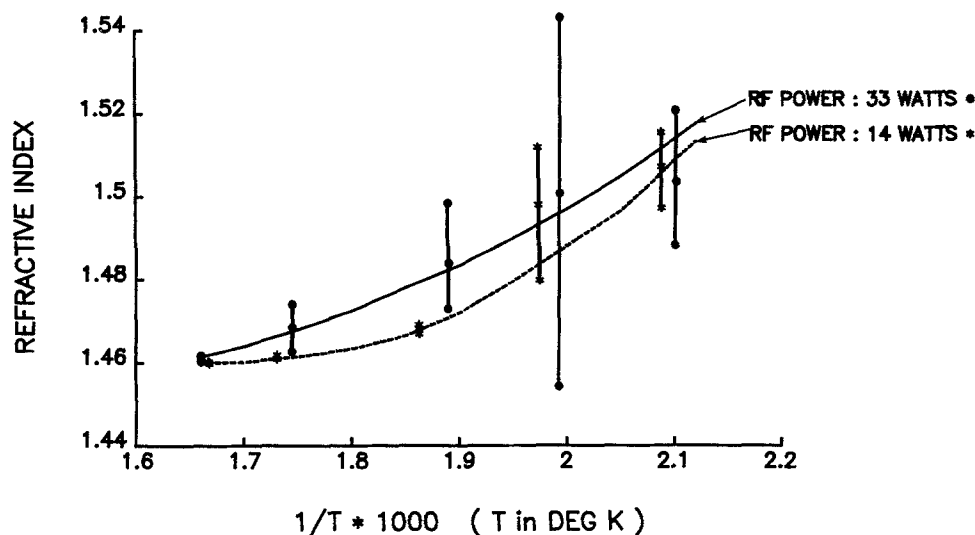


Fig. 5. Variation of refractive index with inverse temperature for the same set of growth conditions as in Fig. 4, curves (c) and (d). The vertical lines represent the spread in the refractive index measured at various points on the substrate.

fects probably accompany the addition of these trace gases, they do cause an increased brightness of the plasma discharge which may be due to either the higher intensity of emission of the Ar and N<sub>2</sub> ionized species compared to O<sub>2</sub> or may result from an enhanced coupling of the RF energy into the plasma. In either case trace gases like Ar and N<sub>2</sub> do enhance the growth rate. Among the gases studied, the O<sub>2</sub>-N<sub>2</sub> mixture gave both the maximum deposition rate as well as layers with refractive index values closest to bulk SiO<sub>2</sub>. It was, as a result, used for most of the experiments.

The total nitrogen flow rate quoted in the paper is then the total N<sub>2</sub> to the deposition chamber including both carrier and diluent gas entering the reactor directly with the silane as well as the N<sub>2</sub> introduced with the oxygen plasma. From Table I it is clearly evident that beyond a certain concentration, adding additional N<sub>2</sub> has little further effect. Ar in contrast, while enhancing the growth rate above that of O<sub>2</sub> alone, particularly for growth on InP, has much less an effect than N<sub>2</sub>. Most noticeable is the equality of the growth rates on InP and Si when N<sub>2</sub> is present in the plasma. Since N<sub>2</sub> was used as the trace gas in the oxygen plasma for the studies reported in this paper, the growth rate results we shall report can in large measure we believe be accepted as valid for growth both on InP and Si. In fact, when data were taken on layers simultaneously grown on both types of substrates, the results agreed within experimental error.

The variation with growth temperature of the refractive index of the SiO<sub>2</sub> films deposited on silicon is shown in Fig. 5 for the same set of conditions as were employed in Fig. 4. As temperature increases the refractive index of the

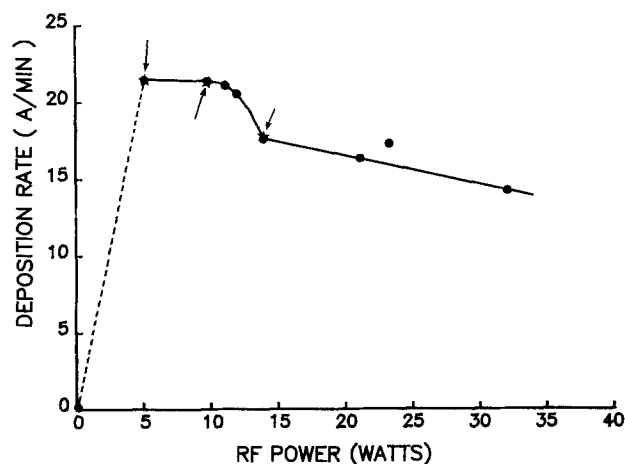


Fig. 6. Deposition rate as a function of RF power input at 253°C and 400 mtorr chamber pressure. Flow rates of gases are the same as in the preceding figures. InP data are indicated by stars and are arrowed.

film asymptotically approaches the refractive index of pure silicon dioxide with a value of 1.46. The vertical bars represent the spread in the refractive index measured over an ~1 in.<sup>2</sup> wafer for a given growth temperature. The spread is low for lower power inputs to the plasma and for high temperatures of growth. The spread increases as temperature decreases and attains a maximum at an intermediate temperature when homogeneous, or gas phase, reaction is seen to occur as was evidenced by the onset of dust formation in the chamber. We attribute the spread in refractive index to nonuniform grain size in the film as the reaction tends towards homogeneous growth. Refractive index values for layers grown on InP showed a much more complex variation with growth conditions in part due presumably to the confounding influence of the non-SiO<sub>2</sub> native oxides of InP underlying the deposited dielectric.

Varying the RF power input to the plasma chamber affects the deposition rate as shown in Fig. 6, where the same set of gas flow conditions was used as for the preceding figures. The deposition rate is negligible for a zero power input and rises sharply to about 22 A/min for a power input of 4W. Based on the geometry of the plasma chamber, and accepting that the plasma is very nonuniformly distributed, we estimate that this corresponds to an average power density of ~9 mW/cm<sup>3</sup> in the discharge. Experimental studies in the range of 0 → 4W power input to the plasma chamber could not be conducted due to the limited resolution of the RF power supply, and in consequence the varia-

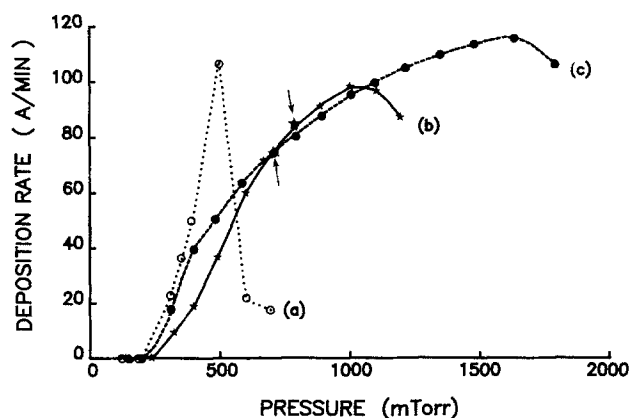


Fig. 7. Effect of pressure on deposition rate. Curve (a): Silane flow rate = 1.95 cm<sup>3</sup>/min, oxygen flow rate = 12 cm<sup>3</sup>/min, nitrogen flow rate = 31 cm<sup>3</sup>/min, RF power = 41W, substrate temperature = 315°C, 3.3 mm ID outlet tube from the plasma chamber. Curve (b): Silane flow rate = 1.28 cm<sup>3</sup>/min, oxygen flow rate = 12 cm<sup>3</sup>/min, nitrogen flow rate = 21.45 cm<sup>3</sup>/min. RF power = 14W, substrate temperature = 253°C, 9.7 mm ID outlet tube from plasma chamber. Curve (c): Conditions same as for curve (b) except chamber temperature = 315°C. InP samples are indicated by larger symbols and arrows.

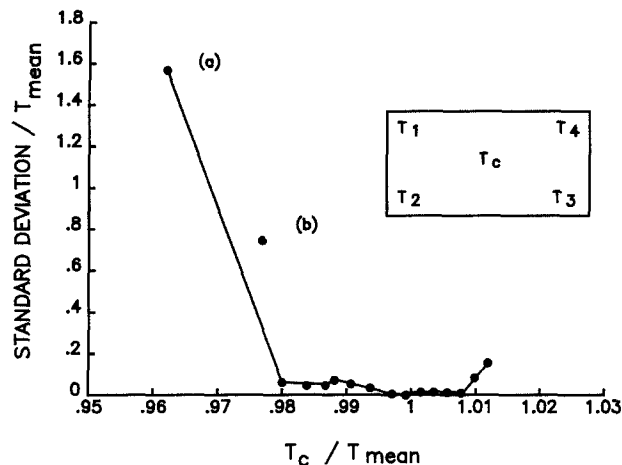


Fig. 8. Thickness spread for various samples measured over an approximately  $2 \text{ cm}^2$  area. All samples were grown under heterogeneous conditions except samples (a) and (b) which were grown at high pressure where gas phase nucleation occurs.

tion in this range is simply represented by a dashed straight line. For the temperature and gas flow conditions of this experiment the presence of the plasma is clearly essential to  $\text{SiO}_2$  growth although the amount of power required is evidently quite small. Following onset of the reaction, growth rates are seen to be constant to  $\sim 10\text{W}$  and then start decreasing. Such a behavior is contrary to most reactions studied in conventional (direct) plasma CVD systems and, as will be discussed later, may result from a number of factors. Figure 7 illustrates the pressure dependence of deposition rate measured at two different temperatures for all other deposition parameters as before. Curves (b) and (c) represent data with the plasma chamber described in the Experimental section using a 9.7 mm ID outlet tube from the plasma chamber to the growth reactor. Curve (a) represents data with a 3.3 mm ID tube. It can be seen that for a given temperature there is a threshold pressure below which no deposition occurs. Above the threshold, deposition rate increases, reaches a peak, and then starts dropping. Beyond the pressure range encompassed by the data in Fig. 7 a homogeneous gas phase reaction occurred as was evidenced by the formation and deposition of particulates in the growth reactor. In this homogeneous growth region the reaction is quite erratic resulting in highly nonuniform and irreproducible growth rates. This is illustrated in Fig. 8 where thickness readings were taken at the four corners and at the center of a number of samples, each measuring  $\sim 2 \text{ cm}^2$  in area.  $T_{\text{mean}}$  is the average of the thicknesses measured at the corners and  $T_c$  is the thickness at the center. One standard deviation nor-

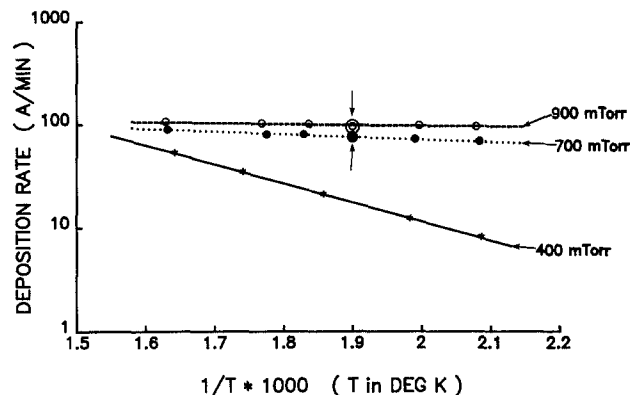


Fig. 10. Arrhenius plot of deposition rate at three different chamber pressures for an RF power input of 14W. Flow rates are the same as in Fig. 7. InP samples are indicated by larger symbols and arrows.

malized by  $T_{\text{mean}}$  is then plotted against  $T_c/T_{\text{mean}}$  for each sample. Most of the data, corresponding to layers grown under heterogeneous conditions, clearly lie very close to  $T_c/T_{\text{mean}} = 1.0$  with low standard deviation. The exception is for the two samples identified as (a) and (b) which are quite nonuniform and were grown in the homogeneous reaction ranges. Excluding these two samples, the data in Fig. 8 correspond to good thickness uniformity with variations  $< 3\%$  over the  $2 \text{ cm}^2$  area of the samples. The composition of the deposits also varied from that of  $\text{SiO}_2$  in the homogeneous growth region as is clear from the decrease in refractive index recorded in Fig. 9. The effect of plasma chamber geometry on the growth rate is also shown in Fig. 7. It can be seen that, for the plasma chamber with the smaller 3.3 mm diameter outlet the curve is shifted to the left, with the increase and decrease in growth rate in this case being very rapid. Figure 10 shows the manner in which the growth rate varies with inverse temperature at three different total pressures for all other parameters being as before. The curve at 400 mtorr repeats the data shown in Fig. 4. Consistent with the results in Fig. 7, the apparent activation energy is seen to decrease with pressure increase approaching almost zero at 900 mtorr.

The preceding data have recorded the variations in growth rate which result as the physical conditions in the reaction chamber are varied. To fully characterize the kinetics of a growth process, it is also necessary to determine its dependence on gas phase composition. The dependence of growth rate on oxygen molar flow rate for two silane concentrations in our system is shown in Fig. 11. For these data, all conditions, including silane flow rate, were held constant, while a sequence of layers were grown at various oxygen flow rates. Growth rates with silane molar

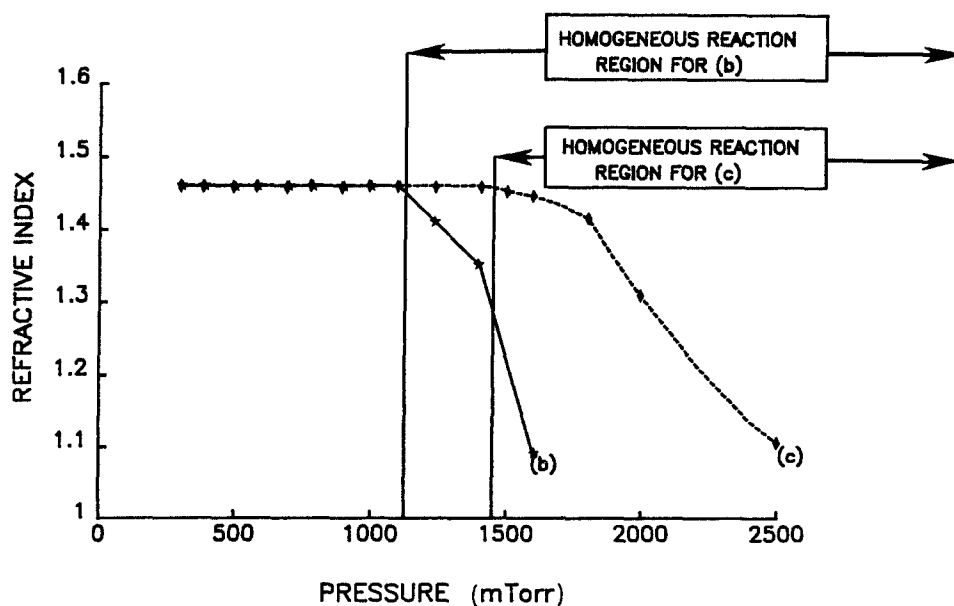


Fig. 9. Variation of refractive index with pressure for samples grown on Si substrates under the experimental conditions of Fig. 7.

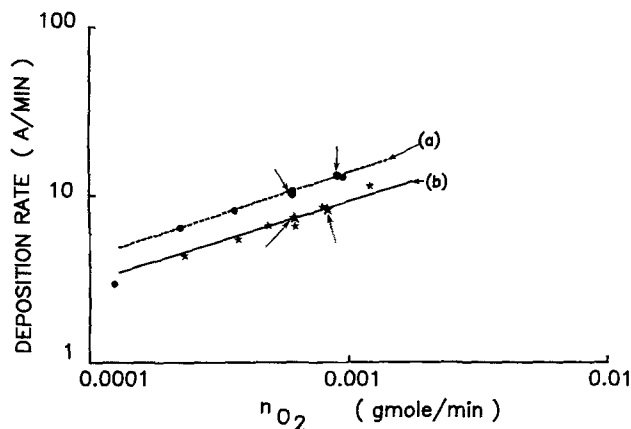


Fig. 11. Deposition rate as a function of oxygen molar concentration with (a) silane concentration = 0.00004 gmol/min, (b) silane concentration = 0.000022 gmol/min, chamber pressure = 400 mtorr, temperature = 253°C, RF power input = 14W. InP samples are indicated by larger symbols and arrows.

flow varying and oxygen concentration remaining constant are shown in Fig. 12. For both sets of data the temperature was maintained constant at 253°C and the total pressure was held at 400 mtorr. The RF power input in all these experiments was 14W. In all cases the growth rate is seen to closely approach a linear function of the gas concentrations when plotted on a log-log scale indicating a power law dependence of rate on both  $\text{SiH}_4$  and  $\text{O}_2$  molar flow rate.

### Discussion

Silicon dioxide films deposited by silane-oxygen reactions using the already outlined remote plasma enhanced technique is potentially a complicated process involving plasma chemistry, homogeneous gas phase reactions, and heterogeneous surface controlled growth. Depending on which values of the key parameters such as temperature, pressure, concentration of reactants, and plasma power are employed, either one, or a combination of these processes could be limiting in determining the resulting film properties. In this section we will discuss the data reported in the previous section and attempt both a self-consistent explanation of the probable controlling reactions as well as develop a model that describes the kinetics of the growth process.

*Addition of nitrogen to the glow discharge.*—It is well known that when mixtures of nitrogen and oxygen are passed through an RF plasma discharge, nitric oxide (NO) is one of the predominant reaction products formed. Previous studies (7) have indicated that the addition of NO to a

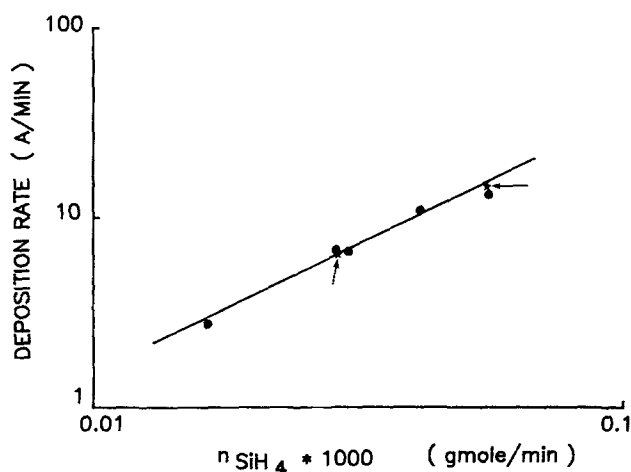
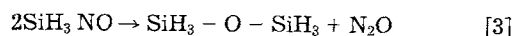
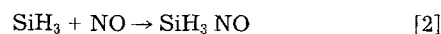
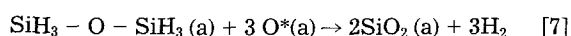
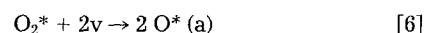


Fig. 12. Effect of silane concentration on deposition rate with oxygen concentration constant at 0.00062 gmol/min, chamber pressure = 400 mtorr, temperature = 253°C, RF power input = 14W. InP samples are indicated by stars and arrows.

monosilane glow discharge completely inhibits the production of  $\text{SiH}_x$  solids and also causes a decrease in the yield of higher polymers of silane. The gaseous products examined by mass spectrometry showed the presence of  $(\text{SiH}_3)_2\text{O}$  and  $\text{N}_2\text{O}$  according to



In light of these results we propose that the deposition of  $\text{SiO}_2$  in our oxygen plasma system is achieved by an initial homogeneous reaction to form the diSilyle ether molecule as already outlined in reactions [1], [2], and [3] and a subsequent terminating heterogeneous surface reaction according to



where "v" represents a vacant site on the substrate surface and (a) is an adsorbed species. In this growth scheme the effect of the plasma is to provide both a source of NO as well as excited species of oxygen in the growth zone and is an explanation for the enhanced effect of  $\text{N}_2$  over trace amounts of Ar for example in the plasma in increasing growth rates. LPCVD of silicon dioxide grown from the  $\text{SiH}_3\text{-NO}$  reaction (8) examined under both thermal and direct plasma excited conditions show an incorporation of  $\text{N}_2$  in the films. In contrast, measurements by AES on our films showed no detectable quantities of  $\text{N}_2$  incorporation which suggests that reactions [2] and [3] are probably occurring in the gas phase. The strong influence of pressure on the growth rate as seen in Fig. 7 also indicates a good likelihood of a heterogeneous component in the overall reaction scheme lending support to the proposed steps [4] through [7].

The growth rate enhancement resulting from the presence of  $\text{N}_2$  in the plasma as documented in Table I could seemingly be due to either or both (i), an increase in atomic oxygen production in the presence of small concentrations of  $\text{N}_2$  in the plasma (9, 10) or (ii), scavenging of all silane by the fast reacting free radical NO via the reaction proposed above. Either of these mechanisms would in turn inhibit both dust formation via gas phase reaction and other polymerization reactions of silane. In contrast, gases such as pure oxygen or ( $\text{O}_2 + \text{Ar}$ ) do not allow the formation of NO in the plasma chamber. Together with decreased availability of atomic oxygen (9, 10) this would be more likely to permit homogeneous reactions, an expectation which is in fact consistent with our observation of some dust formation in the reactor under almost all deposition conditions using these growth gases. Such a decrease in the availability of atomic oxygen would clearly result in a reduction of the surface controlled rate of growth of  $\text{SiO}_2$  in agreement with observation.

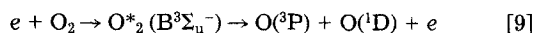
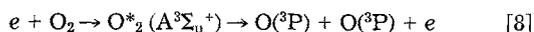
Reactions [2] and [3] can be assumed to take place strongly since  $\text{SiH}_3$  and NO are both free radicals. Our mass spectroscopic results indicate that the amount of NO formed in the plasma chamber for constant  $\text{O}_2$  flow rate, chamber pressure, and RF power does not vary much up to a  $\text{N}_2$  flow rate of  $\sim 8 \text{ cm}^3/\text{min}$  and then starts decreasing slightly as the  $\text{N}_2$  flow rate to the plasma chamber is further increased. We attribute this slight decrease to the geometry and location of the plasma chamber in our experimental setup. As the  $\text{N}_2$  flow rate to the plasma chamber increases, the average pressure in the plasma would be expected to increase leading to the slight decrease in conversion to NO. Increased  $\text{N}_2$  to the plasma above a flow rate of  $\sim 3 \text{ cm}^3/\text{min}$  does not change the growth rate significantly as is shown by the results in Table I.

*Effect of pressure and plasma chamber geometry.*—At very low pressures ( $< 200 \text{ mtorr}$ ), as shown in Fig. 7, there appear to be no reactions occurring either leading to film

deposition or dust formation. No reaction is observed under these pressure conditions even when the power input to the plasma chamber is increased to as high as 50W, the gas flow rates changed, or the temperature increased to 375°C. Furthermore, the plasma tube diameter does not seem to affect the threshold pressure although, as can be seen in Fig. 7, increasing temperature does reduce the growth threshold slightly. Although processes occurring in the plasma discharge at low pressures are quite complex, we believe the near zero deposition rate at low pressures is due to the unavailability of atomic oxygen in the reaction zone. Experimental results by Sabadil (11) on plasma electron density variation with pressure show a decrease in electron density approaching zero for sufficiently reduced pressures. A decrease in pressure results both in an enhancement of the loss of electrons through diffusion and an increase of the mean free path which decreases the collision frequency, two effects which together result in a decrease in dissociation rate. An additional effect of the pressure reduction is the increase in heterogeneous recombination rate on the walls of the plasma chamber and in the tube leading to the growth chamber due to an increase in gas velocity. This probably results in the reaction zone being totally devoid of atomic oxygen.

The drop in growth rate at high pressures may result from a number of factors. Energy transferred in electron-molecule collisions is less if the mean free path of electrons is reduced as results, for example, from an increase in pressure. The rate constant for inelastic collisions is thus reduced, shifting the electron energy distribution to lower values. In bimolecular reactions, since the rate is proportional to total pressure, the growth rate increases due to an enhancement in reaction rate and then drops because of lower electron energy. An increase in pressure also tends to favor three body homogeneous recombination reactions (12) causing a further decrease in reaction rate at higher pressures. At an even higher pressure the onset of homogeneous reaction is marked by dust formation in the reaction chamber. This probably is due to gas phase nucleation that is promoted by the increased gas phase collisions. Films deposited under these conditions are hazy with a very low refractive index, as shown in Fig. 9, probably due to a porous structure. The shift in growth rate peaks towards lower pressure with a smaller ID plasma tube outlet, as shown by the data in Fig. 7, is likely due to the larger pressure drop experienced in such a tube. With the experimental setup described previously, for a constant reactor pressure, the pressure in the smaller tube would be somewhat higher than for a larger diameter tube. This shifts the balance of rate enhancement due to the pressure increase and rate decrease due to loss of atomic oxygen and three body recombination reactions towards lower pressures as seen in Fig. 7. It is however difficult to interpret the actual peak deposition rates due to changes in the two experimental conditions.

**Plasma power density.**—Molecular oxygen can be excited from its ground state either to the  $A^3\Sigma_u^+$  or  $B^3\Sigma_u^-$  state by electron collision expressed as (12)



It is presumably to be expected for our proposed reaction scheme that for a given silane flow rate the deposition rate would be proportional to the oxygen atom concentration and NO concentration. As the power to the plasma chamber is increased the rate of dissociation increases and hence more oxygen atoms are formed. This is shown in Fig. 6 in the deposition rate increase observed for powers up to about 4W.

The rate of three body recombination reactions (13)

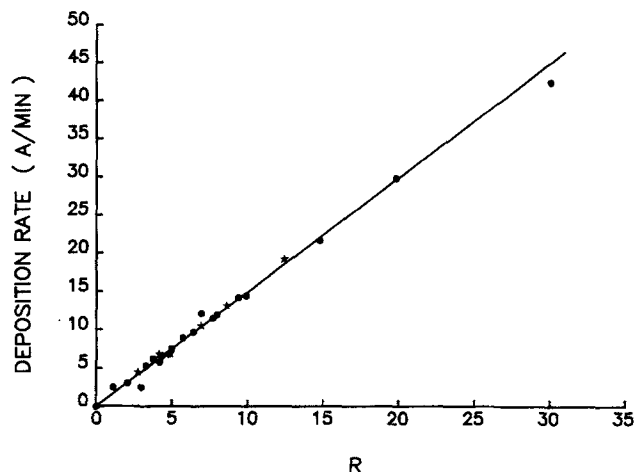
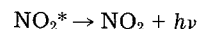


Fig. 13. Plot of deposition rate for all samples studied at 400 mtorr and an RF power input of 14W as a function of  $R$ . InP samples are indicated by stars.

is proportional to the concentration of oxygen atoms present. The decrease in the deposition rate with further increase in power beyond  $\sim 10W$  shown in Fig. 6 could thus be due to the loss of oxygen atoms by recombination reactions. An added effect in causing the decrease in the deposition rate is the increase in gas temperature and the plasma chamber wall temperature as the RF power is increased. An increase in both these temperatures enhances the heterogeneous rate of recombination of oxygen atoms thereby decreasing the deposition rate.

Mass spectrometer measurements in our system reveal an increase in NO concentration as the plasma power is increased for constant  $N_2$  and  $O_2$  flow rates. Conversion to NO was in the order of 1  $\rightarrow$  3% for the experimental conditions studied. Loss of oxygen atoms or NO through the reverse reaction



can be discounted since it is relatively slow (9, 14). Hence the loss of atomic oxygen through heterogeneous and homogeneous recombination reactions and the subsequent drop in growth rate more than offsets increases in NO concentration or other reactions which accompany increase in plasma power.

The preceding discussion has presented a possible reaction scheme for the growth of  $SiO_2$  from silane and oxygen. Irrespective of the details of the reaction however it is evident from the data shown in Fig. 11 and 12 that the deposition rate proceeds as a power law in  $[O_2]$  and  $[SiH_4]$  and moreover, for growth at 400 mtorr total pressure and 14W of RF power, the process exhibits an activation energy from Fig. 4 of  $8.4 \pm 0.6$  kcal/mol.

Combining these various dependencies we can express the overall kinetics for the  $SiH_4-O_2, N_2$  reaction as follows

$$DR = 1.4R \quad [15]$$

where  $R = \exp(-4227/T) \cdot (n_{O_2})^{0.5} (n_{SiH_4})^{1.6} \times 10^{13}$ ,  $DR$  is the deposition rate in  $\text{\AA}/\text{min}$ ;  $T$  is the temperature in K;  $n_{O_2}$  is the oxygen molar flow rate in  $\text{gmol}/\text{min}$ ;  $n_{SiH_4}$  is the silane molar flow rate in  $\text{gmol}/\text{min}$ .

The precision of this relationship in describing the reaction is illustrated in Fig. 13, where we have replotted all the deposition rate data shown in Fig. 4-12, including growth on Si and InP substrates, as a function of  $R$ . The scatter in the data about a linear dependence is very small, corresponding to a correlation coefficient of 0.98.

#### Acknowledgment

The financial assistance of NASA Lewis in support of this work is gratefully acknowledged.

Manuscript submitted Jan. 29, 1987; revised manuscript received Oct. 9, 1987.

Colorado State University assisted in meeting the publication costs of this article.

## REFERENCES

1. S. V. Nguyen, *J. Vac. Sci. Technol.*, **B4(5)**, 1159 (1986).
2. S. Matsuo and M. Kiuchi, *Jpn. J. Appl. Phys.*, **22**, 210 (1983).
3. J. W. Peters, F. L. Gebhart, and T. C. Hall, *Solid State Technol.*, **9**, 121 (1980).
4. L. G. Meiners, *J. Vac. Sci. Technol.*, **21**, 655 (1982).
5. P. D. Richard, R. J. Markunas, G. Lucovsky, G. G. Fountain, A. N. Mansour, and D. V. Tsu, *ibid.*, **A3**, 867 (1985).
6. R. E. Logar, M. T. Wauk, and R. S. Rosler, in "Sixth International Conference on Chemical Vapor Deposition," L. F. Donaghey, P. Rai-Choudhury, and R. N. Tauber, Editors, p. 195, The Electrochemical Society Softbound Proceedings Series, PV 77-5, Princeton, NJ (1977).
7. P. A. Longeway, R. D. Estes, and H. A. Weakliem, *J. Phys. Chem.*, **88**, 73 (1984).
8. J. G. Wilkes, *J. Cryst. Growth*, **70**, 271 (1984).
9. F. Kaufman and J. R. Kelso, *J. Chem. Phys.*, **32**, 301 (1960).
10. F. K. McTaggart, "Plasma Chemistry in Electrical Discharges," p. 148, Elsevier, New York (1967).
11. H. Sabadil, *Beitr. Plasma Phys.*, **53** (1971).
12. A. T. Bell, in "Techniques and Applications of Plasma Chemistry," J. R. Hollahan and A. T. Bell, Editors, p. 46, Wiley, New York (1974).
13. A. T. Bell and K. Kwong, *AIChE J.*, **18**, 990 (1972).
14. F. Kaufman, *Proc. Royal Soc.*, **A247**, 123 (1959); *J. Chem. Phys.*, **28**, 352 (1958).

## Convection and Mass-Transport in Laser-Induced Chemical Vapor Deposition

S. Patnaik\* and R. A. Brown

Department of Chemical Engineering and Materials Processing Center, Massachusetts Institute of Technology, Cambridge, Massachusetts 02139

## ABSTRACT

Gas flow and energy and species transport in laser-induced chemical vapor deposition (LICVD) of amorphous silicon films by silane pyrolysis are analyzed by finite element analysis of a two-dimensional model for the process. Spatial non-uniformity of the deposited film is shown to result from diffusion controlled transport of products between the beam and substrate. Deposition profiles are affected by buoyancy-driven convection only at increased gas pressures. Horizontal orientation of the reactor with respect to gravity is optimal because the stagnation-like flow, that results adjacent to the substrate, enhances mixing, and smoothes the film profile.

Laser-assisted chemical vapor deposition is becoming increasingly more common in semiconductor device fabrication. The spatial coherence and monochromaticity of the laser beam cause localized heating and photoassisted chemical reaction, which produce high spatial resolution of the deposited film. Most of the early laser assisted processes (1-3) directed the beam perpendicular to the substrate to create a localized hot spot on the substrate while some researchers (4, 5) tuned the lasing frequency so that the gas and substrate were heated simultaneously resulting in deposition as small surface features. Laser-induced chemical vapor deposition (LICVD) is a relatively new process which has been used to produce large area amorphous, hydrogenated silicon films (a:Si-H) (6-8). This paper describes a modeling study of the transport processes important in the LICVD process.

A prototype of a LICVD system for deposition from silane is shown schematically in Fig. 1. Reactant gas is introduced at low pressure, typically on the order of 10 torr, and passed over a substrate placed on a heated block and maintained at a temperature between 300° and 450°C. An infrared CO<sub>2</sub> laser used in a CW mode and tuned to the absorption spectrum of the gas is passed parallel to the substrate. The reactant gas absorbs photons from the laser and decomposes by thermal pyrolysis to produce radicals and reactive intermediates. These products are transported to the substrate by diffusion and convection and deposit via surface driven reactions to form the film.

LICVD offers a tremendous advantage over conventional techniques for amorphous film growth in that it allows independent control of the gas and substrate temperatures. The decomposition of silane and the growth rate of the film are controlled by the energy input from the laser, and are relatively unaffected by the substrate temperature (9). The temperature of the substrate controls film forming reactions that result in deactivation of adsorbed film precursors and hydrogen evolution from the surface

and thereby determine the electrical properties of the material (10). Low substrate temperatures lead to sufficient hydrogen incorporation resulting in defect passivation and improved electrical properties, while the gas temperature can be increased independently to enhance the growth rate.

The unique thermal configuration of a LICVD reactor also affects transport processes in the system and the spatial uniformity of the grown film. Because LICVD employs relatively cold reactor walls it is not subject to the parasitic reactions, contamination, and depletion effects which plague reactors with hot walls. However, large temperature gradients exist between the bulk gas and the walls which can lead to buoyancy-driven convection in the system. Convective species transport caused by gas motion should lead to asymmetry in the deposition profile, with the direction and magnitude of the skewness dependent on the orientation of the substrate relative to gravity. The plot of film thickness along the substrate shown as Fig. 3.4 in Ref. (11) has the reflective symmetry about the center of the laser beam expected for diffusion dominated species transport; these results indicate the free convection is probably suppressed near the substrate for the low gas pressure (~10 torr) used in these experiments.

The resulting nonuniformity in film thickness, which is over 100% between the center (point closest to the beam) and the edge of the film, is unacceptable. One of the aims of this work is to use detailed analysis of heat, mass, and species transport to examine the possibility of using convective transport to improve the spatial uniformity and compositional homogeneity of the film. Prediction of diffusive and convective transport requires analysis of heat and mass transport for a compressible, multi-component gas, accounting for forced flow through the LICVD reactor and buoyancy-driven convection. Models for these processes and the finite-element/Newton algorithm used for solution are presented in the next section.

Prediction of the film composition requires models for both the gas phase and surface kinetics important in the

\*Electrochemical Society Student Member.